Journal of Molecular Structure 1004 (2011) 271–283

Contents lists available at SciVerse ScienceDirect

Journal of Molecular Structure

journal homepage: www.elsevier.com/locate/molstruc

Synthesis, spectroscopic characterization, pH-metric and thermal behavior on Co(II) complexes formed with 4-(2-pyridyl)-3-thiosemicarbazide derivatives

T.A. Yousef [a], O.A. El-Gammal [b], S.E. Ghazy [b], G.M. Abu El-Reash [b,*]

[a] Department of Toxic and Narcotic Drug, Forensic Medicine, Mansoura Laboratory, Medicolegal Organization, Ministry of Justice, Egypt
[b] Department of Chemistry, Faculty of Science, Mansoura University, Mansoura 35516, Egypt

ARTICLE INFO

Article history:
Received 25 June 2011
Received in revised form 7 August 2011
Accepted 8 August 2011
Available online 24 August 2011

Keywords:
Thiosemicarbazide
PM3
Co complexes
Coats–Redfern
Horowitz–Metzger
pH-metry

ABSTRACT

Four new cobalt (II) complexes of some thiosemicarbazides have been synthesized and spectrochemically characterized. The thiosemicarbazides are prepared by the addition of 4-(2-pyridyl)-3-thiosemicarbazide to phenyl isothiocyanate (H_2PPS), benzoyl isothiocyanate (H_2PBO), phenyl isocyanate (H_2APO) and 2-pyridyl isothiocyanate (H_2PPY). The complexes are characterized by elemental analysis, spectral (IR, ^1H NMR and UV–Vis), thermal and magnetic measurements. The studies revealed that structures of complexes are of two types octahedral and tetrahedral. The octahedral complexes are of H_2PPS, which acts as di-anionic tetradentate SSNN and H_2APO acts as mono-anionic tridentate NON. The tetrahedral complexes are of H_2PBO, which acts as di-anionic tridentate NSO and H_2PPY acts as mono-anionic bidentate NS. From the modelling studies, the bond length, bond angle, HOMO, LUMO and dipole moment had been calculated to confirm the geometry of the ligands and their investigated complexes. From TG and DTA studies kinetic parameters are determined using Coats–Redfern and Horowitz–Metzger methods. From pH metric studies at 298, 303 and 308 K and μ (0.1, 0.15 and 0.2) in 50% dioxane–water mixture the protonation constants of the ligands, the stepwise stability constants of the complexes and their thermodynamic parameters are calculated.

1. Introduction

Heterocyclic thiosemicarbazones have aroused considerable interest in chemistry due to their remarkable coordination properties and in biology owing to a wide spectrum of potential biological activities [1–4]. The biological activity of thiosemicarbazone complexes is related to its chelating ability toward the transition metal ions, whether the bonding through nitrogen, and sulfur atoms [4] or oxygen, nitrogen and sulfur atoms [5–7]. The activity of heterocyclic thiosemicarbazones is affected by the presence of N(4) substitution [8,9]. We report here the preparation of Co(II) complexes of N^1-phenyl-N^2-(pyridin-2-yl)hydrazine-1,2-bis(carbothioamide) (H_2PPS), N-phenyl-2-(2-(pyridin-2-ylcarbamothioyl) hydrazinyl)-2-thioxoacetamide (H_2PBO), N-phenyl-2-(pyridin-2-ylcarbamothioyl)hydrazinecarboxamide (H_2APO) and 1-(aminoN-(pyridin-2-yl)methanethio)-4-(pyridin-2-yl)thiosemicarbazide (H_2PPY) with study the substituent effect on the thiosemicarbazidic moiety and its coordination behavior. Also, the thermal degradation kinetic parameters such as energy of activation (E_a) and the pre-exponential factor (A) and thermodynamic parameters like entropy (ΔS), enthalpy (ΔH) and activation energy (ΔG) for each step of degradation have been evaluated.

2. Experimental

2.1. Instrumentation and materials

All the chemicals were purchased from Aldrich and Fluka and used without further purification. Elemental analyses (C and H) were performed with a Perkin–Elmer 2400 series II analyzer. IR spectra (4000–400 cm^{-1}) for KBr discs was recorded on a Mattson 5000 FTIR spectrophotometer. Electronic spectra were recorded on an Unicam UV–Vis spectrophotometer UV2. Magnetic susceptibilities were measured with a Sherwood scientific magnetic susceptibility balance at 298 K. ^1H NMR measurements in d_6-DMSO at room temperature was carried out on a Varian Gemini WM-200 MHz spectrometer at the Microanalytical Unit, Cairo University. Thermogravimetric measurements (TGA, DTA, 20–800 °C) were recorded on a DTG-50 Shimadzu thermogravimetric analyzer at a heating rate of 10 °C/min and nitrogen flow rate of 20 ml/min.

2.2. Synthesis of the ligands

4-(2-Pyridyl)-3-thiosemicarbazide was synthesized as reported earlier [10]. Derivatives 1–4 were prepared by boiling ethanolic solution of 4-(2-pyridyl)-3-thiosemicarbazide (1.6 g, 100 mmol) with an equimolar amount of phenyl isothiocyanate, benzoyl isothiocyanate, phenyl isocyanate and 2-pyridyl isothiocyanate Fig. 1.

* Corresponding author. Tel.: +20 100373155; fax: +20 502219214.
E-mail address: gaelreash@mans.edu.eg (G.M. Abu El-Reash).

0022-2860/$ - see front matter Crown Copyright © 2011 Published by Elsevier B.V. All rights reserved.
doi:10.1016/j.molstruc.2011.08.020

2.3. Synthesis of metal complexes

All complexes were prepared by refluxing H_2PPS, H_2PBO, H_2APO or H_2PPY (1.0 mmol) and $CoCl_2{\cdot}6H_2O$ (1.0 mmol) in 30 ml ethanol for 2–3 h. The solid complexes were filtered off, washed with ethanol followed by diethyl ether and dried in a vacuum over $CaCl_2$.

2.4. Procedure for the pH-metric titration

The pH-metric readings were measured to 0.01 unit with Orion's research model 601A/digital Ionalyzer standardized before and checked after each titration with buffer solutions produced by Fischer (New Jersey, USA). The following mixtures were prepared and titrated potentiometrically at 298, 303 and 308 K against 9.2×10^{-3} M NaOH in 50% (v/v) dioxane–water at a constant ionic strength KCl (0.1, 0.15 and 0.2 M). The solution mixtures (i–iii) were prepared as follows:

(i) 1.25 ml (1.1×10^{-2} M) HCl + 1.25 ml (0.1, 0.15 and 0.2 M) KCl + 10 ml doubly-distilled H_2O.
(ii) 1.25 ml (1.1×10^{-2} M) HCl + 1.25 ml (0.1, 0.15 and 0.2 M) KCl + 2.5 ml (5×10^{-3} M) H_2PPS, H_2PBO, H_2APO and H_2PPY + 10 ml bi-distilled H_2O.
(iii) 1.25 ml (1.1×10^{-2} M) HCl + 1.25 ml (0.1, 0.15 and 0.2 M) KCl + 2.5 ml (5×10^{-3} M) H_2PPS, H_2PBO, H_2APO and H_2PPY + 0.5 ml (5×10^{-3} M) Co^{2+} in bi-distilled water + 9.5 ml H_2O.

The ultimate volume (25 ml) was adjusted by adding dioxane in each case and after adding of each increment of the titrant, the solution was stirred for about two minutes and the pH-reading is then recorded. For converting the pH-meter reading (B) in 50% (v/v) dioxane–water and 0.1, 0.15 and 0.2 M KCl to $[H^+]$ values, the equation of Van Uitert and Hass [11] was applied,

$$-\log[H^+] = B + \log U_H$$

where $\log U_H$ is the correction factor for the solvent composition and ionic strength for which B is read.

2.5. Molecular modeling

An attempt to gain better insight on the molecular structure of the ligand and its complexes, geometric optimization and conformational analysis has been performed using PM3 [12] forcefield as implemented in hyperchem 8 [13]. The low lying obtained from MM+ was then optimized at PM3 using the Polak–Ribiere algorithm in RHF–SCF, set to terminate at an RMS gradient of 0.01 kcal mol^{-1}.

3. Results and discussion

The physical and analytical data of each ligand and their Cobalt complexes are listed in Table 1.

3.1. Infrared and ^1H NMR spectra of ligands

The most important IR bands of ligands are recorded in Table 2. The spectra exhibit three bands between 3234 and 3100 cm^{-1} due to ν(NH) groups. The ν/δ modes of (CN) group of pyridyl ring are found at ≈1560 and 620–635 cm^{-1}.

An inspection on the Table 2 describing the IR spectra of H_2PPS, H_2PBO, and H_2PPY indicates that the appearance of strong bands assigned to ν(C=N) (azomethine), ν(C—S) and ν(SH) as well as (C=S) modes suggested that these ligands exist in thione–thiol form. As these ligands contain two C=S groups, $(C{=}S)^1$ and $(C{=}S)^2$, we proposed that $(C{=}S)^1$ is in thione form and $(C{=}S)^2$ in thiol form. This assumption is confirmed by the absence of bands due to ν(C=N) (azomethine), ν(C—S) and ν(SH) vibrational modes in the IR spectrum of the start (4-pyridyl thiosemicarbazide) [14] and the missing of SH signal in the ^1H NMR spectrum of H_2APO.

In the IR spectrum of H_2PPY, the band due to ν(C=N) mode was difficult to recognize because it is overlapped with ν(C=C) of pyridyl ring. Furthermore, the appearance of ν(C—S) at higher wavenumber, 683 cm^{-1} than that of other ligands may be due to the presence of pyridyl groups at the extremes of H_2PPY structure, which act as electron withdrawing groups. The IR spectrum of H_2APO exhibits a sharp band at 3521 cm^{-1} due to ν(OH) in addition to the ν(CO) band at 1675 cm^{-1} suggested the keto–enol tautomerism.

The ^1H NMR spectra of H_2PPS, H_2PBO and H_2PPY (Figs. 2–4) derivatives in DMSO-d6 show two signals at approximately δ=11.10 and 15.4 ppm relative to TMS that disappear upon adding D_2O. These signals are attributed to the amide ($NH_{a,a'}$) and thiol (SH) protons. The signal at δ = 8.29 ppm is due to the (NH_b), while the multiplets at 7.00–7.86 ppm are characteristic of the pyridine ring protons [15]. The appearance of signal at δ 15.4 ppm in the

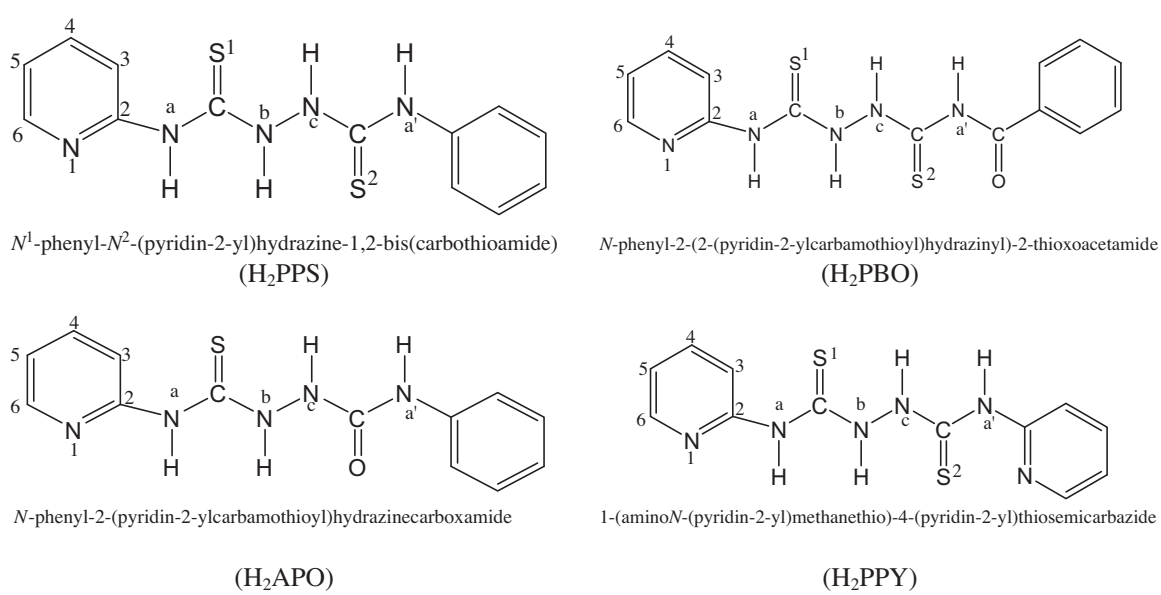

Fig. 1. Structure of H_2PPS, H_2PBO, H_2APO and H_2PPY.

Table 1
Analytical and physical data of H_2PPS, H_2PBO, H_2APO, H_2PPY and their Co(II) complexes.

Compound		Color	M.p. (°C)	Found (Calcd.)%				Yield (%)
Empirical formula	(F.Wt)			M	Cl	C	H	
H_2PPS		Yellow	180	–	–	51.33	4.19	93
$C_{13}H_{13}N_5S_2$	(303.41)					(51.46)	(4.32)	
$[Co(PPS)(H_2O)_2](H_2O)$		Dark	>300	14.1	–	37.91	4.35	89
$C_{13}H_{17}CoN_5O_3S_2$	(414.36)	Brown		(13.9)		(37.68)	(4.14)	
H_2PBO		Yellow	270	–	–	50.81	3.88	90
$C_{14}H_{13}N_5OS_2$	(331.42)					(50.74)	(3.95)	
$[Co(PBO)(H_2O)](H_2O)_2$		Dark	>300	13.5	–	37.75	3.59	88
$C_{14}H_{17}CoN_5O_4S_2$	(442.39)	Green		(13.3)		(38.0)	(3.87)	
H_2APO		White	182	–	–	54.51	4.43	90
$C_{13}H_{13}N_5OS$	(287.27)					(54.35)	(4.56)	
$[Co(HAPO)Cl(H_2O)_2](H_2O)$		Dark	>300	13.29	8.47	35.59	4.03	90
$C_{13}H_{18}CoN_5O_4SCl$	(436.69)	Green		(13.6)	(8.15)	(35.76)	(4.15)	
H_2PPY		Yellow	310	–	–	47.47	4.55	93
$C_{12}H_{12}N_6S_2$	(304.35)					(47.31)	(3.97)	
$[Co(HPPY)Cl(H_2O)](H_2O)$		Green	>300	14.1	8.6	33.85	3.25	85
$C_{12}H_{16}CoN_6O_2S_2Cl$	(433.83)			(13.6)	(8.2)	(33.19)	(3.48)	

Table 2
Assignments of the IR spectral bands of H_2PPS, H_2PBO, H_2PBO, H_2PPY and their Co(II) complexes.

Compound	$\nu(NH)^{a,a'}$	$\nu(NH)^{b,c}$	$\nu(C{=}N)_{py}$	$\nu(C{=}N)^*$	$\nu(C{=}S)$	$\nu(C{=}N)$	$\delta(C{=}N)_{py}$	$\nu(N{-}N)$	$\nu(C{=}O)$	$\nu(C{-}O)$	$\nu(OH)$	$\nu(SH)$	$\nu(C{-}S)$
H_2PPS	3160,3099	3220	1562	–	860	1646	624	971	–	–	–	–	660
$[Co(PPS)(H_2O)_2](H_2O)$	3133	3258	–	1540	–	1616	643	1006	–	–	–	–	635
H_2PBO	3118	3228	1562	–	861	1641	630	990	1672	1164	3337	–	660
$[Co(PBO)(H_2O)](H_2O)_2$	3129	–	1562	–	–	1621	620	1008	–	1206	–	2390	634
H_2APO	3158	3239	1542	–	865	–	634	1008	1675	1243	3363	–	–
$[Co(HAPO)Cl(H_2O)_2](H_2O)$	–	3262	1527	1563	–	1626	670	1043	–	1216	–	2380	620
H_2PPY	3174	3234	1562	–	861	–	625	1000	–	–	–	–	683
$[Co(HPPY)Cl(H_2O)](H_2O)$	3126	–	1565	1629	–	1620	595	1006	–	–	–	2380	630

spectrum of H_2PPY due to SH proton and a signal at δ 12.57 ppm due to OH group in the spectrum of H_2APO (Fig. 5) confirms the thiol–enol tautomerism in solution.

3.2. Infrared spectra of complexes

A careful comparison of the IR spectra of ligands and their Co(II) complexes in Table 2 gave a good insight on the mode of bonding and the nature of metal–ligand bond. The IR spectra of the polymer $[Co(PPS)(H_2O)_2](H_2O)$ complex showed that H_2PPS behaves as binegative tetradentate *via* two thiol (C—S) and two azomethine nitrogen groups Fig. 6.

H_2PBO acts as binegative tridentate through the $(C{=}N)^*$, (C=S) that adjacent to N^c substitutent (i.e. phenyl group) in thiol form and enolized (C—O) groups Fig. 7.

H_2APO acts as mononegative tridentate coordinating *via* $(C{=}N)_{py}$, enolized (C—O) and $(C{=}N)^*$ groups Fig. 8.

Finally, H_2PPY behaves as mononegative bidentate through $(C{=}N)_{py}$ and one of (C=S) groups in thiol form Fig. 9.

This is supported by the following:

(i) Disappearance of bands due to $\nu(NH)_{b,c}$ and (C=S) modes with appearance of new bands at 1540, 1563 and 630, 635 cm^{-1} attributable to (C=N—N=C) and (C—S) vibrations in the IR spectra of $[Co(PPS)(H_2O)_3]$ and $[Co(PBO)(H_2O)](H_2O)_2$ complexes, respectively.

(ii) The clear shift of the band due to $\nu(C{=}N)$ of free ligands H_2PPS and H_2PBO at 1641 and 1646 cm^{-1} to a lower wavenumber (1616 and 1621 cm^{-1}) in their complexes is consistent with coordination of the azomethine nitrogen to the central Co(II) atoms, which is further supported by the increase in frequency of the hydrazinic N—N bond as a consequence of the reduction between the lone pairs of electrons on the hydrazine nitrogen atoms. Additional evidence for coordination of the imine nitrogen is the presence of a band at 449 cm^{-1} due to ν(Co—N) vibration falling in the 435–450 cm^{-1} range for the divalent metal centers [16].

(iii) The pyridine in-plane deformation mode at 625–634 cm^{-1} in the spectra of the ligands shifts to 620–621 cm^{-1} in the IR spectra of the above complexes, suggesting coordination of the heteroaromatic nitrogen [17–20].

(iv) The disappearance of ν(C—OH) band in the cobalt complexes of $[Co(PBO)(H_2O)](H_2O)_2$ and $[Co(HAPO)Cl(H_2O)_2](H_2O)$ suggests its coordination with displacement of proton. The shift of ν(C—O) to higher wavenumber confirms the suggested behavior for these ligands. In addition the bands at 540 and 553 cm^{-1}, respectively due to ν(M—O) reveals this coordination.

3.3. Electronic spectra and magnetic moments

The electronic spectral features of ligands and their complexes in DMF and Nujol mull are summarized in Table 3.

The spectrum of $[Co(PPS)(H_2O)_2](H_2O)$ exhibited two strong bands at 18,050 and 19,084 cm^{-1} while of $[Co(HAPO)Cl(H_2O)_2](H_2O)$ at 14,925 and 14,577 cm^{-1}. These bands corresponding to $^4T_{1g}(F) \rightarrow {}^4T_{1g}(P)$ and $^4T_{1g}(F) \rightarrow {}^4A_{2g}(F)$ transitions [21,22] arising from the high-spin d^7 configuration Co(II) in an octahedral geometry.

Finally, the green complexes, $[Co(HPPY)Cl(H_2O)](H_2O)$ and $[Co(HPBO)(H_2O)_2]$ exhibit an intense bands at 14,553 and 25,381 cm^{-1} for the first complex and at 14,662 and 23,697 cm^{-1} for the second assignable to the $^4A_2(F) \rightarrow {}^4T_1(P)$ and $^4A_2(F) \rightarrow {}^4T_2(F)$ transitions. The shoulders at 16,722 cm^{-1} and at 16,393 cm^{-1} due to spin coupling [21] respectively, confirming a tetrahedral geometry for these complexes.

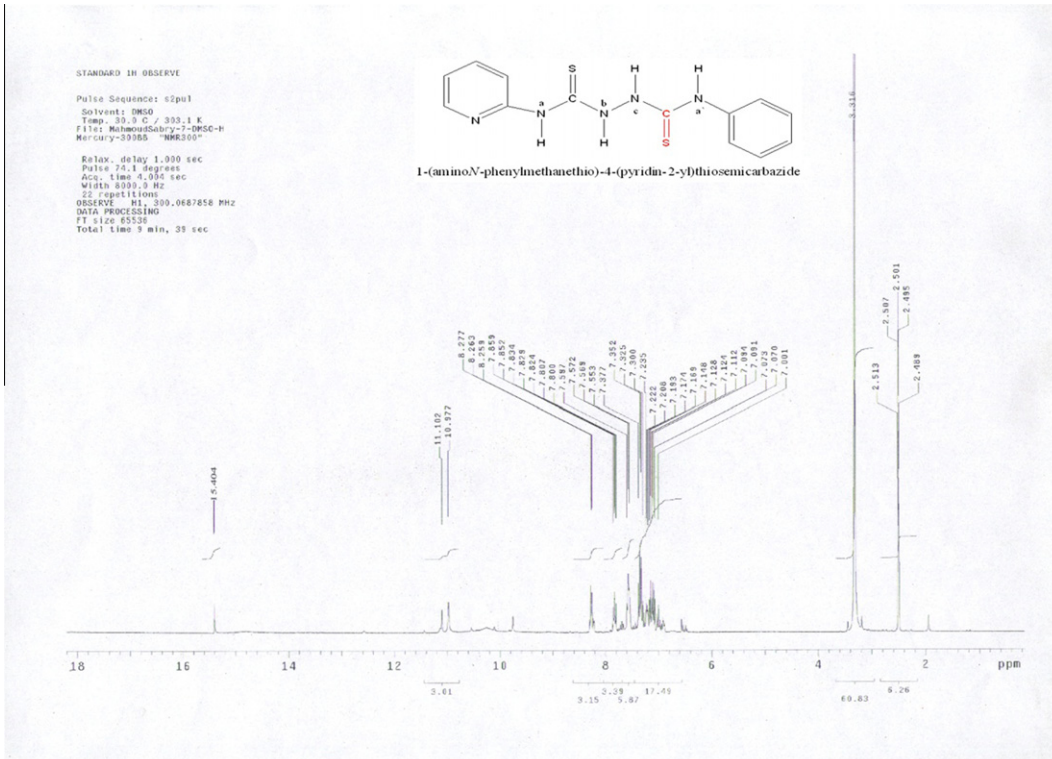

Fig. 2. ^{1}H NMR spectrum of H_2PPS.

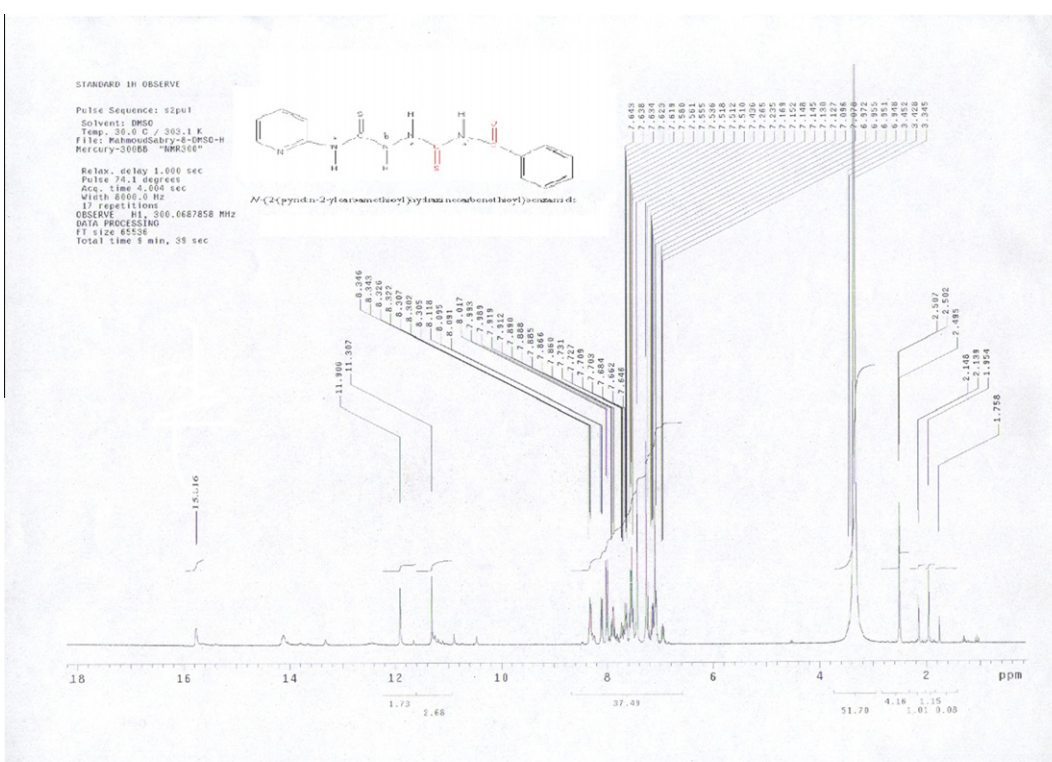

Fig. 3. ^{1}H NMR spectrum of H_2PBO.

3.4. Molecular modeling

The molecular structure along with atom numbering of Co(II) complexes are shown in Figs. 2–4.

Analysis of the data in Tables 1S–14S (Supplementary materials) calculated for the bond lengths and angles for the bond. One can conclude the following remarks:

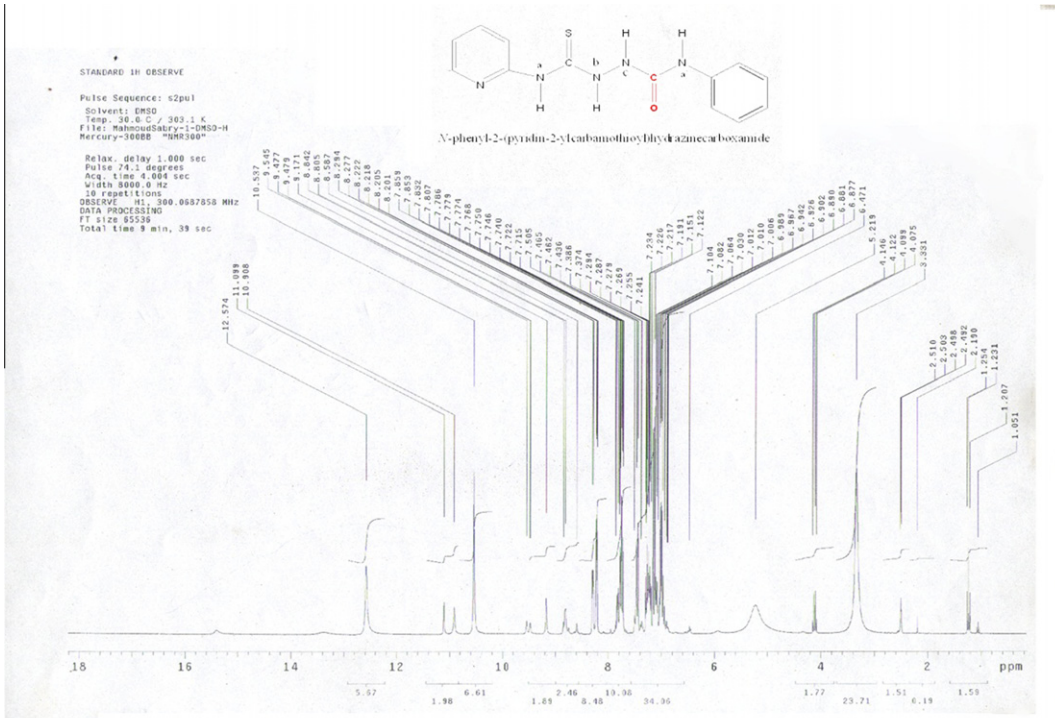

Fig. 4. ^{1}H NMR spectrum of H_2APO.

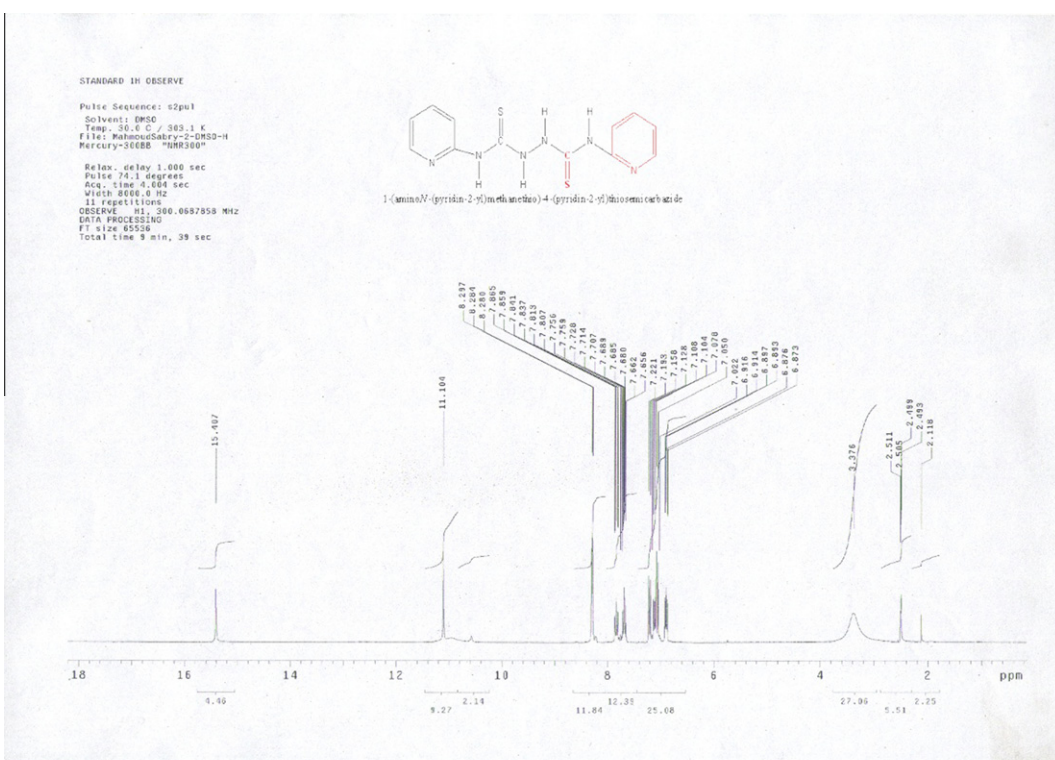

Fig. 5. ^{1}H NMR spectrum of H_2PPY.

1. The bond angles of the thiosemicarbazide moiety are altered somewhat upon coordination; the largest change affects N(10)—N(11)—C(12) and C(12)—N(14)—C(15) angles which are reduced from 124° and 121.4° on ligand to 100.9° and 112.2° in case of [Co(HPBO)(H_2O)$_2$] complex, C(5)—C(4)—N(7) and N(7)—C(8)—S(9) from 126.6° and 128.8° on ligand to 117°

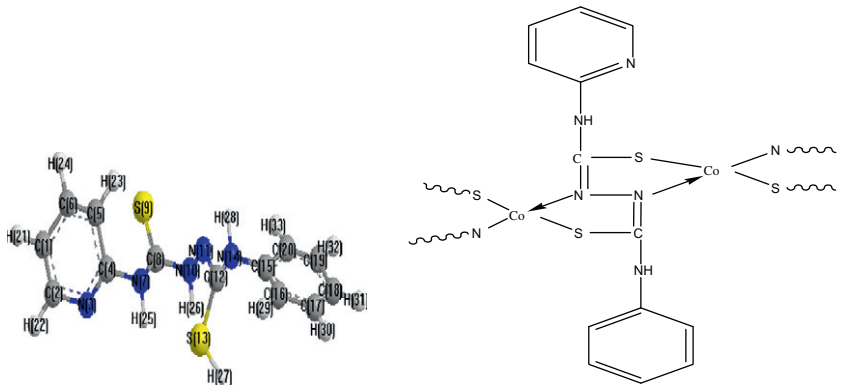

Molecular modeling of H_2PPS [Co(PPS)(H_2O)$_2$](H_2O) complex

Fig. 6. Molecular modeling of H_2PPS and [Co(PPS)(H_2O)$_2$](H_2O) complex.

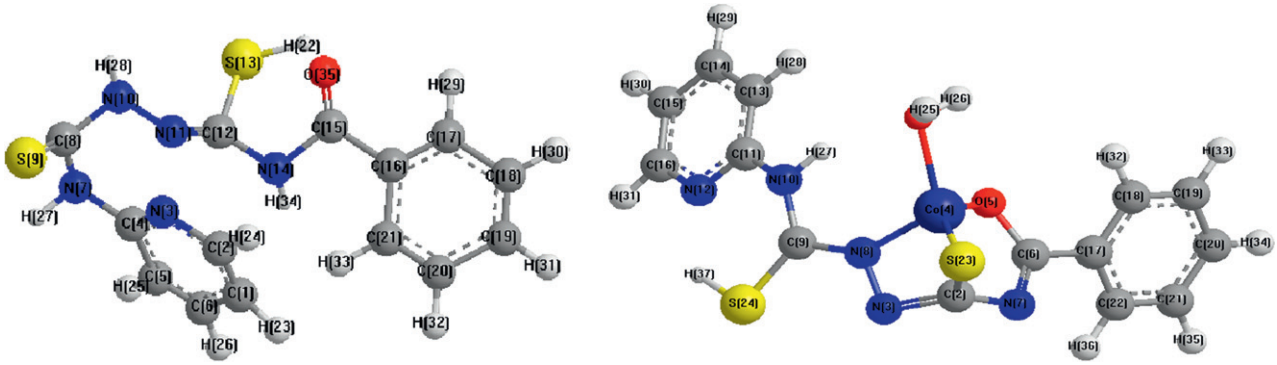

Molecular modeling of H_2PBO Molecular modeling [Co(PBO)(H_2O)](H_2O)$_2$ complex

Fig. 7. Molecular modeling of H_2APO and molecular modeling of [Co(HAPO)Cl(H_2O)$_2$](H_2O) complex.

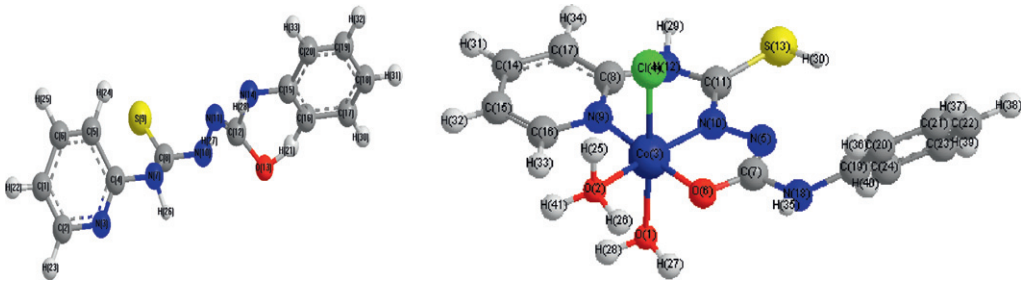

Molecular modeling of H_2APO Molecular modeling of [Co(HAPO)Cl(H_2O)$_2$](H_2O) complex

Fig. 8. Molecular modeling of H_2APO and molecular modeling of [Co(HAPO)Cl(H_2O)$_2$](H_2O) complex.

and 112.6° in case of [Co(HAPO)Cl(H_2O)$_2$](H_2O) complex and N(11)—C(12)—S(13) from 123.6° on ligand to 130.4° in case of [Co(HPPY)Cl(H_2O)](H_2O) as a consequence of bonding.

2. All bond angles in [Co(PBO)(H_2O)](H_2O)$_2$ and [Co(HPPY)Cl(H_2O)](H_2O) complexes are quite near to a tetrahedral geometry predicting sp^3 hybridization while for [Co(PPS)(H_2O)$_2$](H_2O) and [Co(HAPO)Cl(H_2O)$_2$](H_2O), which have octahedral geometry predicting sp^3d^2 hybridization.
3. All the active groups taking part in coordination have bonds longer than that already exist in the ligand (like C=S, N—H, $(C{=}N)_{py}$ and C=O) especially C(8)—N(10) from 1.42–1.45 Å to 1.31–1.33 Å

The lower HOMO energy values of H_2PBO and H_2PPY show that molecule donating electron ability is the weaker. On contrary, the higher HOMO energy implies that the molecule is a good electron donor. LUMO energy presents the ability of a molecule receiving electron as in Table 15S [22].

3.5. Thermogravimetric studies

The stages of decomposition, temperature range, decomposition product as well as the found and calculated weight loss percentages of the complexes are given in Table 4. In most complexes, the first decomposition step representing the elimination of water of hydration.

3.6. Kinetic data

Non-isothermal calculations were used extensively to evaluate the thermodynamic and kinetic parameters for the different thermal

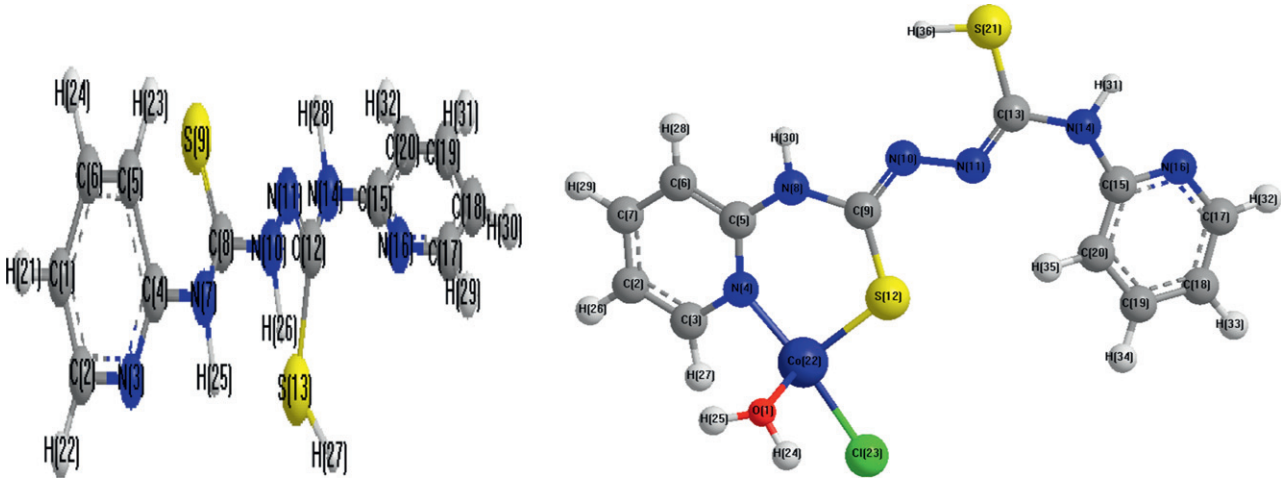

Fig. 9. Molecular modeling of H_2PPY and molecular modeling of $[Co(HPPY)Cl(H_2O)](H_2O)$ complex.

Table 3
Magnetic moment, electronic bands and ligand field parameters of the Co(II) complexes of H_2PPS, H_2PBO, H_2PBO and H_2PPY.

Compound	Solvent	Band position (cm^{-1})	Dq	B	β	μ_{eff} (B.M.)
H_2PPS	DMF	35,211 31,847 29,069	–	–	–	–
	Nujol	–	–	–	–	
$[Co(PPS)(H_2O)_2](H_2O)$	DMF	35,211 31,055 25,773 18,050 14,925	782.7	815.3	0.84	3.18
	Nujol	24,390 22,321 19,762 17,857 16,556	774.3	806.5	0.83	
H_2PBO	DMF	35,461 32,680 29,070	–	–	–	–
	Nujol	–	–	–	–	
$[Co(PBO)(H_2O)](H_2O)_2$	DMF	35,211 29,940 24,510 18,797	815	849	0.87	2.9
	Nujol	23,697 20,161 18,305 16,393 14,662	793.8	826.8	0.85	
H_2APO	DMF	35,211 32,051	–	–	–	–
	Nujol	–	–	–	–	
$[Co(HAPO)Cl(H_2O)_2](H_2O)$	DMF	35,211 32,467 22,624 19,084 16,835 14,577	827	862	0.89	3.1
	Nujol	26,178 23,364 18,797 14,837	815	849	0.87	
H_2PPY	DMF	35,211 30,120 18,050	–	–	–	–
	Nujol	–	–	–	–	
$[Co(HPPY)Cl(H_2O)](H_2O)$	DMF	35,211 31,847 29,585 25,126 19,157 16,667 14,706	317.5	721.5	0.74	3.91
	Nujol	25,381 19,380 16,722 14,535	313.8	713.1	0.73	

decomposition steps of the Co(II) complexes were determined using the Coats–Redfern [23] and Horowitz–Metzger [24].

The rate of decomposition of a solid depends upon the temperature and the amount of material. The expression for the thermal decomposition of a homogeneous system has the following general form:

$$\frac{d\alpha}{dt} = K(T)g(\alpha) \tag{1}$$

where t is the time, T is the absolute temperature and α is the degree of transformation defined as:

$$\alpha = \frac{w_o - w_t}{w_o - w_\infty}$$

In which w_o, w_t and w_∞ are the weights of the sample before the degradation, at temperature t and after total conversion, respectively. $K(T)$ is the rate coefficient that usually follows the Arrhenius equation. The differential conversion function, $g(\alpha)$ may present various functional forms but its most commonly form for solid-state reactions is $g(\alpha) = (1 - \alpha)n$, where n is the reaction order, assumed to remain constant during the reaction [25,26].

The rate constant is normally expressed by the Arrhenius equation:

$$K = A\exp\left(-\frac{E_a}{RT}\right) \tag{2}$$

where E_a is the activation energy, A is the Arrhenius pre-exponential factor which indicates how fast the reaction occurs and R is the gas constant in (J mol^{-1} K). Substituting in Eq. (1), we get:

$$\frac{d\alpha}{dt} = A\exp\left(-\frac{E_a}{RT}\right)g(\alpha) \tag{3}$$

When the reaction is carried out under a linear temperature program ($T = T_o + \beta t$, where $\beta = dT/dt$ is the heating rate and T_o the

Table 4
Decomposition steps with the temperature range and weight loss for ligands and their cobalt complexes.

Compound	Temp. range (°C)	Removed species	Wt. loss	
			Found%	Calcd%
H_2PPS	141–228	—Py + NH	30.84	30.68
	229–371	—Py + NH + CS	45.76	45.18
	513–691	—N_2H_2	9.58	9.8
	691–800	CS (residue)	13.8	14.5
$[Co(PPS)(H_2O)_2](H_2O)$	32–115	—H_2O	4.34	4.35
	176–300	—$2H_2O$	9.35	8.7
	300–392	—$C_5H_4 + N_4 + C_2 + H$	36.29	35.02
	392–582	—NH + C_6H_5	22.37	22.23
	582–800	Co + 2S (residue)	30.2	29.7
H_2PBO	0–210	—Py + NH	28.58	28.09
	210–370	$C_3H_3S_2O$	48.16	48.64
	370–700	C_6H_5	23.28	23.27
$[Co(PBO)(H_2O)](H_2O)_2$	44–115	—$2H_2O$	8.27	8.14
	290–483	—H_2O + Py + $N_3H_2 + C_2$ + S	44.15	44.36
	483–716	—N + C_7H_5	22.77	23.31
	716–800	CoO + S (residue)	24.81	24.19
H_2APO	126–217	—$C_5H_5N_2 + N_2H_2$	42.15	42.85
	217–344	—C_6H_5 + CO + NH	41.11	41.82
	344–700	CS (residue)	16.74	15.34
$[Co(HAPO)Cl(H_2O)_2](H_2O)$	10–78	—H_2O	4.42	4.13
	78–274	—$2H_2O$ + Cl	16.9	16.37
	274–387	—Py + NH + C + HN_2	30.48	30.71
	387–574	—C_6H_5 + NH + C	23.9	23.84
	574–700	CoO + S (residue)	24.3	24.5
H_2PPY	188–246	—N_2H_2	10.57	9.86
	246–400	—2Py + N_2H_2	60.96	61.18
	400–700	2CS (residue)	28.78	28.96
$[Co(HPPY)Cl(H_2O)](H_2O)$	30–157	—H_2O	4.28	4.15
	157–296	—H_2O	5.35	4.15
	296–376	—Cl + NH + N	15.5	14.86
	376–471	—Py	17.64	17.99
	471–595	—NH + 2C + NH + Py	30.1	30.46
	595–700	Co + 2S (residue)	27.13	28.28

starting temperature). A large number of decomposition processes can be represented as first order reaction [27]. Particularly, the degradation of the investigated series of metal complexes was suggested to be first order in sample weight reaction. Therefore we will assume $n = 1$ for the remainder of the present text. Under this assumption the integration of Eq. (3) leads to:

$$\ln(1-\alpha) = -\frac{A}{\beta}\int_{T_o}^{T} \mathrm{Exp}\left(\frac{E}{RT}\right)dT \tag{4}$$

On the basis of Eq. (4), it is possible to analyze experimental data by the integral method, in order to determine the degradation kinetic parameters A, E_a. The temperature integral in the right-hand side of Eq. (4) has no exact analytical solutions and several kinds of approximations are generally used. Two methods that differ on the way of resolving Eq. (4) are compared using the TGA data of the studied complexes. These methods are:

3.6.1. Coats–Redfern method

The Coats–Redfern [23] method is as follows:

$$\ln\left[\frac{g(\alpha)}{T^2}\right] = \ln\left(\frac{AR}{\beta E}\right) - \frac{E_a}{RT} \tag{5}$$

where $g(\alpha) = 1 - (1-\alpha)1 - n/1 - n$ for $n \neq 1$ and $g(\alpha) = -\ln(1-\alpha)$ for $n = 1$, R is the universal gas constant. The correlation coefficient, r, was computed using the least square's method for different values of n (n = 0.33, 0.5, 0.66 and $n = 1$) by plotting $\ln[\frac{g(\alpha)}{T^2}]$ versus 1/T for the investigated metal complexes are shown in Fig. 10. The n-value which gave the best fit ($r \approx 1$) was chosen as the order parameter for the decomposition stage of interest. The slope of the straight line equal (E_a/R) and the intercept the pre-exponential factor, A can be determined. The data obtained are represented in Table 5.

3.6.2. Horowitz–Metzger method

The Horowitz–Metzger [24] relation was used to evaluate the degradation kinetics is

$$\ln[-\ln(1-\alpha)] = \frac{E_a\theta}{RT_S^2} \quad \text{for } n = 1 \tag{6}$$

$$\ln\left[\frac{1-(1-\alpha)^{1-n}}{1-n}\right] = \ln\left(\frac{A}{\beta}\frac{RT_S^2}{E}\right) - \frac{E_a}{RT_S} + \frac{E_a\theta}{RT_S^2} \quad \text{for } n \neq 1 \tag{7}$$

where $\theta = T - Ts$, Ts is the DTG peak temperature, T the temperature corresponding to weight loss Wt. In this method a straight line should be observed between $\ln[\ln(1-\alpha)]$ and θ with a slope of $\frac{E_a}{RT_S^2}$.

Fig. 11 show the Horowitz–Metzger plots for the metal complexes under study. The obtained data are recorded in Table 6.

3.6.3. Thermodynamic parameters

The other thermodynamic parameters of activation can be calculated by Eyring equation [28,29]:

$$\Delta H^* = E_a - RT \tag{8}$$

$$\Delta S^* = R\left(\ln\frac{hA}{K_B T} - 1\right) \tag{9}$$

$$\Delta G^* = \Delta H - T\Delta S \tag{10}$$

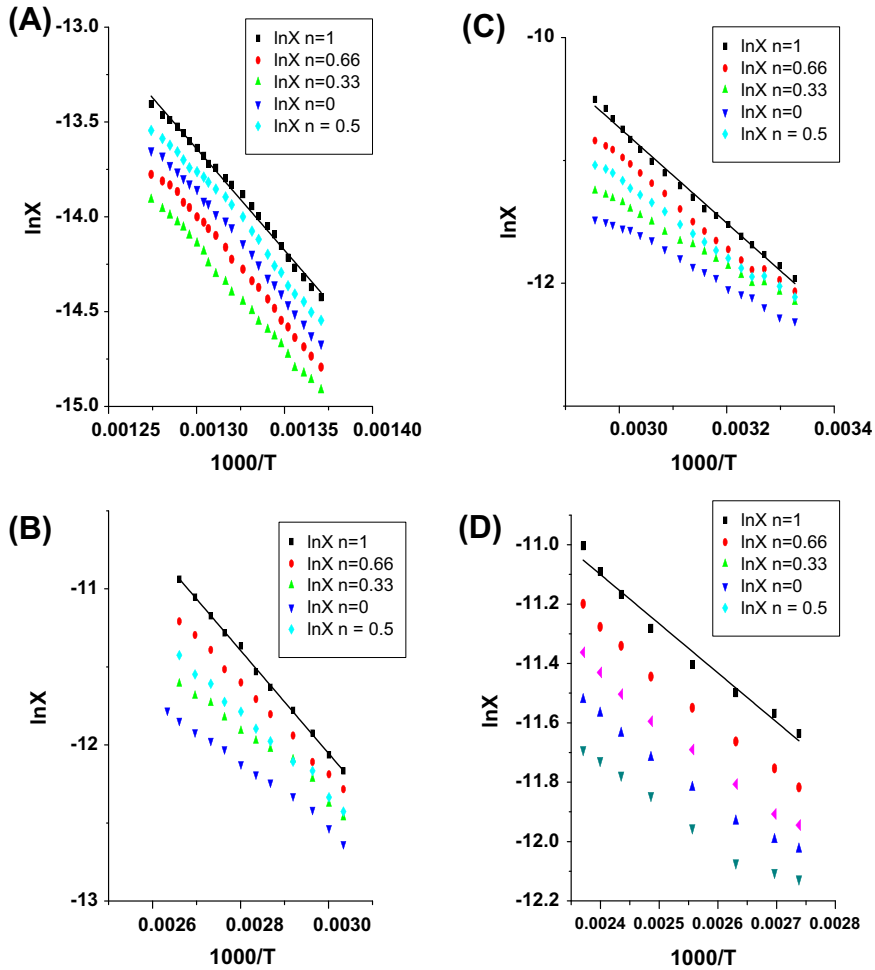

Fig. 10. Coats–Redfern plots of (A) $[Co(PPS)(H_2O)_2](H_2O)$, (B) $[Co(PBO)(H_2O)](H_2O)_2$, (C) $[Co(HAPO)Cl(H_2O)_2](H_2O)$ and (D) $[Co(HPPY)Cl(H_2O)](H_2O)$.

where ΔH^* is the enthalpy of activation (kJ/mol), ΔS the entropy of activation (kJ/mol K) and ΔG^* the Gibbs free enthalpy of activation (kJ/mol), h the Planck constant and K_B the Boltzmann constant. The kinetic parameters evaluated by Coats–Redfern and Horowitz–Metzger methods are listed in Tables 5 and 6, respectively. From the results obtained, the following remarks can be pointed out:

(i) All decomposition steps show best fit for $n = 1$.
(ii) The negative value of the entropy of activation, ΔS^* of some decomposition steps in case of the ion exchanger and its metal complexes with all investigated metal ions indicates that the activated fragments have more ordered structure than the undecomposed ones and the later are slower than the normal [30,31].
(iii) The positive sign of activation enthalpy change, ΔH^* indicates that the decomposition stages are endothermic processes.
(iv) The high values of the energy of activation, E_a of the complexes reveals the high stability of such chelates due to their covalent bond character [32].
(v) The positive sign of ΔG^* for the investigated complexes reveals that the free energy of the final residue is higher than that of the initial compound, and hence all the decomposition steps are nonspontaneous processes. Moreover, the values of ΔG^* increase significantly for the subsequent decomposition steps of a given compound. This results from increasing the $T\Delta S^*$ clearly from one step to another which override the values of ΔH^* reflecting that the rate of removal of the subsequent species will be lower than that of the precedent one [33–35]. This may be attributed to the structural rigidity of the remaining complex after the expulsion of one or more ligands, as compared with the precedent complex, which requires more energy, $T\Delta S^*$, for its rearrangement before undergoing any decomposition change.

3.7. Potentiometric metric studies

The potentiometric measurements were carried out according the procedure developed by Clavin and Bjerrum [36,37].

3.7.1. Determination of the proton–ligand ionization constants

The ionization constants of H_2PPS, H_2PBO, H_2APO and H_2PPY were determined pH-metrically using Irving–Rossotti technique at (298, 303 and 308 K) and at constant ionic strength of ($\mu = 0.1$, 0.15 and 0.2 M KCl). The free acid (0.011 M) and its mixture with the ligand (0.0005 M) were titrated against carbonate-free sodium hydroxide (0.0092 M) solution. The titration curves for ligands are shown in Figs. 1S–4S respectively.

The average number of protons associated with the ligand, $\bar{n}_A$ was calculated at different pH-values using Irving–Rossotti equation [38].

The proton–ligand ionization curves, obtained by plotting $\bar{n}_A$ versus pH at different temperature are shown in the Figs. 5S–8S. From these curves, the maximum $\bar{n}_A$ value is found to be ~2 indicating that the investigated ligands have two dissociable protons of the enolized hydrogen ion of NH_b and NH_c respectively.

Table 5
Kinetic parameters of ligands and their cobalt complexes evaluated by Coats–Redfern equation.

Compound	Peak	Mid temp (K)	E_a (kJ/mol)	A (S^{-1})	ΔH^* (kJ/mol)	ΔS^* (kJ/mol K)	ΔG^* (kJ/mol)
H_2PPS	1st	447	94.10	1.2406E−5	90.38	−0.3422	243.24
	2nd	572	118.72	6.2067E−6	113.96	−0.3500	314.20
	3rd	864	129.03	7.5270E−6	121.85	−0.3518	425.76
$[Co(PPS)(H_2O)_2](H_2O)$	1st	346	33.65	1.1907E−5	30.77	−0.3404	148.61
	2nd	511	73.77	1.6481E−6	69.52	−0.3601	253.70
	3rd	620	279.8	5.3642E−6	274.73	−0.3519	492.87
	4th	761	190.0	3.8043E−6	183.70	−0.3564	454.83
H_2PBO	1st	379	42.51	1.0950E−6	39.36	−0.3610	176.17
	2nd	565	50.04	1.3166E−6	45.34	−0.3628	250.39
$[Co(PBO)(H_2O)](H_2O)_2$	1st	351	30.17	3.15944	27.24	−0.2367	110.56
	2nd	638	97.38	2.30197E6	92.07	−0.1485	186.96
	3rd	841	147.06	1.87037E6	140.06	−0.1334	252.40
H_2APO	1st	447	193.17	3.5313E−5	189.45	−0.3335	338.43
	2nd	550	71.05	2.4248E−5	66.48	−0.3383	252.63
$[Co(HAPO)Cl(H_2O)_2](H_2O)$	1st	318	25.16	1.5483E−5	22.52	−0.3375	129.74
	2nd	452	48.19	2.2100E−6	44.43	−0.3566	205.54
	3rd	604	198.17	4.6809E−6	193.14	−0.3528	406.41
H_2PPY	1st	490	224.02	6.1209E−6	219.94	−0.3488	390.95
	2nd	598	122.65	5.5964E−7	117.68	−0.3703	339.22
$[Co(HPPY)Cl(H_2O)](H_2O)$	1st	366	16.83	1.5898E−6	13.79	−0.3576	144.86
	2nd	503	62.73	1.7970E−6	58.55	−0.3592	239.08
	3rd	609	216.26	3.1089E−6	211.19	−0.3562	428.28
	4rd	698	104.33	1.6301E−6	98.53	−0.3627	351.64
	5rd	807	267.26	9.6117E−7	260.55	−0.3683	557.86

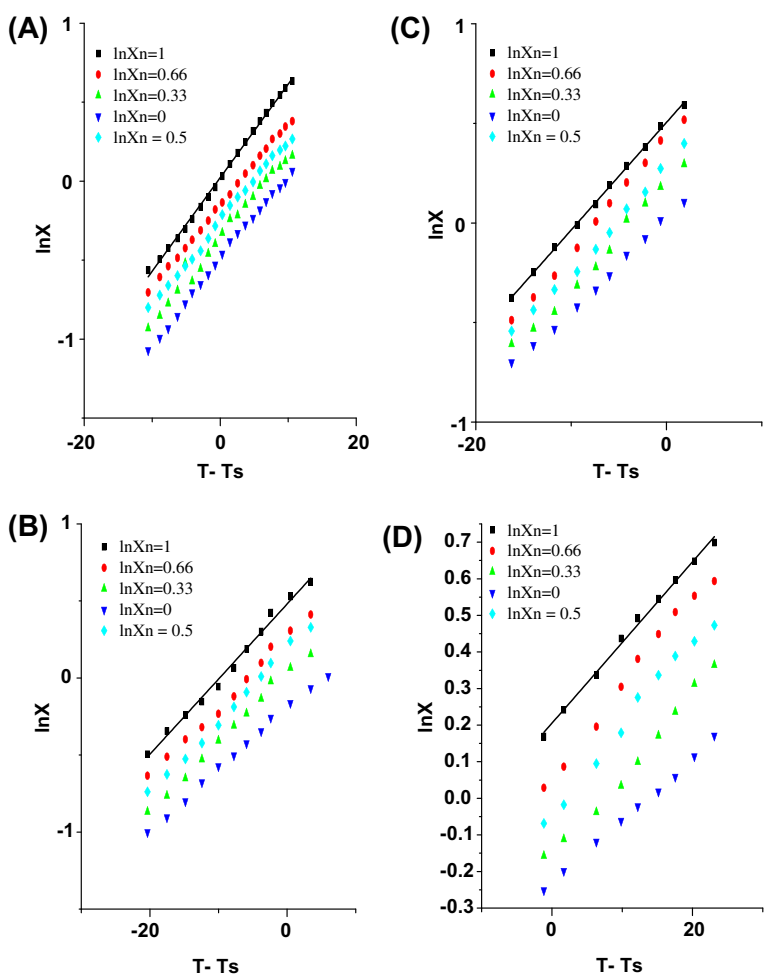

Fig. 11. Horowitz–Metzger plots of (A) $[Co(PPS)(H_2O)_2](H_2O)$, (B) $[Co(PBO)(H_2O)](H_2O)_2$, (C) $[Co(HAPO)Cl(H_2O)_2](H_2O)$ and (D) $[Co(HPPY)Cl(H_2O)](H_2O)$.

Table 6
Kinetic parameters of ligands and their cobalt complexes evaluated by Horowitz–Metzger equation.

Compound	Peak	Mid temp (K)	E_a (kJ/mol)	A (S^{-1})	ΔH^* (kJ/mol)	ΔS^* (kJ/mol K)	ΔG^* (kJ/mol)
H_2PPS	1st	447	94.10	1.2406E−5	90.38	−0.3422	243.24
	2nd	572	118.72	6.2067E−6	113.96	−0.3500	314.20
	3rd	864	129.03	7.5270E−6	121.85	−0.3518	425.76
$[Co(PPS)(H_2O)_2](H_2O)$	1st	346	33.52	1.124E−5	30.64	−0.3409	148.64
	2nd	511	73.51	1.528E−6	69.26	−0.3607	253.77
	3rd	620	279.62	5.330E−6	274.47	−0.3519	492.64
	4th	761	190.47	3.785E−6	184.15	−0.3565	455.30
H_2PBO	1st	379	42.51	1.0950E−6	39.36	−0.3610	176.17
	2nd	565	50.04	1.3166E−6	45.34	−0.3628	250.39
$[Co(PBO)(H_2O)](H_2O)_2$	1st	351	31.10	5.977	28.17	−0.2314	109.63
	2nd	638	97.71	1.5811E5	92.40	−0.1517	189.28
	3rd	841	143.00	4.2788E5	136.00	−0.1457	258.66
H_2APO	1st	447	193.17	3.5313E−5	189.45	−0.3335	338.43
	2nd	550	71.05	2.4248E−5	66.48	−0.3383	252.63
$[Co(HAPO)Cl(H_2O)_2](H_2O)$	1st	318	25.48	1.4979E−5	22.84	−0.3377	130.15
	2nd	452	48.64	2.2297E−6	44.88	−0.3565	205.95
	3rd	604	198.27	4.5854E−6	193.25	−0.3529	406.62
H_2PPY	1st	490	224.02	6.1209E−6	219.94	−0.3488	390.95
	2nd	598	122.65	5.5964E−7	117.68	−0.3703	339.22
$[Co(HPPY)Cl(H_2O)](H_2O)$	1st	366	16.62	1.5925E−6	13.58	−0.3576	144.64
	2nd	503	62.58	1.6449E−6	58.41	−0.3599	239.31
	3rd	609	216.37	2.8629E−6	211.30	−0.3569	428.81
	4rd	698	104.69	1.4482E−6	98.89	−0.3637	352.69
	5rd	807	267.41	9.6035E−7	260.70	−0.3683	558.02

Table 7
The dissociation constants of H_2PPS in 50% (V/V) dioxane–water and KCl at different temperatures and it's thermodynamic parameters.

μmol/L	Dissociation constant						Free energy change (ΔG) kJ mol^{-1}						Enthalpy change (ΔH) kJ mol^{-1}	Entropy change (ΔS) J mol^{-1} K^{-1}	
	298 K		303 K		308 K		298 K		303 K		308 K				
	pK_1	pK_2	pK_1	pK_2	pK_1	pK_2									
0.1	13.45	8.25	12.89	8.15	8.72	6.76	82.7	24.8	83.3	25.0	83.9	25.2	43.37	13.66	−131.9	−37.55
0.15	13.44	10.2	11.98	8.56	11.8	7.88	26.1	21.7	26.3	39.9	27.5	40.2	15.06	21.29	−37.12	−61.28
0.2	12.90	7.80	10.88	7.26	9.25	4.35	63.2	60.9	63.7	61.4	64.2	61.9	33.50	31.63	−99.57	−98.30

Table 8
The dissociation constants of H_2PBO in 50% (V/V) dioxane–water and KCl at different temperatures and it's thermodynamic parameters.

μmol/L	Dissociation constant						Free energy change (ΔG) kJ mol^{-1}						Enthalpy change (ΔH) kJ mol^{-1}	Entropy change (ΔS) J mol^{-1} K^{-1}	
	298 K		303 K		308 K		298 K		303 K		308 K				
	pK_1	pK_2	pK_1	pK_2	pK_1	pK_2									
0.1	12.89	8.99	10.51	8.15	10.02	7.60	48.9	22.8	49.3	23.0	51.9	23.2	26.35	12.77	−75.58	−33.89
0.15	12.98	9.02	11.6	8.55	11.57	7.36	22.0	27.7	22.2	27.9	22.3	28.2	12.94	15.22	−30.46	−42.00
0.2	12.49	7.52	10.46	7.41	9.80	6.48	45.7	16.8	46.0	16.9	46.4	17.1	24.69	9.53	−70.41	−24.44

Table 9
The dissociation constants of H_2APO in 50% (V/V) dioxane–water and KCl at different temperatures and it's thermodynamic parameters.

μmol/L	Dissociation constant						Free energy change (ΔG) kJ mol^{-1}						Enthalpy change (ΔH) kJ mol^{-1}	Entropy change (ΔS) J mol^{-1} K^{-1}	
	298 K		303 K		308 K		298 K		303 K		308 K				
	pK_1	pK_2	pK_1	pK_2	pK_1	pK_2									
0.1	14.00	8.48	13.54	8.04	10.98	6.03	51.2	42.4	27.7	42.7	51.9	43.0	27.67	22.46	−78.75	−66.85
0.15	13.65	9.05	10.81	8.33	9.93	5.30	64.2	66.4	64.7	66.9	65.2	67.4	34.14	34.73	−100.9	−106.2
0.2	13.36	8.64	9.60	7.41	9.41	6.64	68.5	34.2	69.1	34.4	69.6	34.7	36.25	18.36	−108.3	−53.04

The first proton–ligand stability constant (pK_1) for all ligands was determined by interpolation at half-$\bar{n}_A$ values, i.e. at $\bar{n}_A = 0.5$ from the $\bar{n}_A$—pH curves. The second proton-ligand stability constant (pK_2) for all ligands was determined using mid point method, where 2pH ($\bar{n}_A = 1$) = pK_1 + pK_2.

3.7.1.1. Effect of substituent. A glance at Tables 7–10 reveals the order of the ionization constants of the thiosemicarbazides as, H_2APO > H_2PPS > H_2PPY > H_2PBO. This can be explained on the basis of the formation of an intramolecular hydrogen bond [39]. In all cases such thiosemicarbazides the geometry of their molecules is

such to allow the C=S, C=O, (C=N) pyridine and NH groups to be oriented in close proximity to each other. Consequently, it is difficult to lose H^+ so pK is high. ON substituting carbonyl group by thione group, pK value decreased as oxygen is more electronegative than sulfur atom. Also, the presence of pyridyl group in H_2PPY (i.e. electron withdrawing group) will decrease the electron density by its high negative inductive effect, withdrawing electrons more effectively than phenyl group so the stronger is the hydrogen bond and consequently the smaller the pK value.

3.7.1.2. Effect of ionic strength. By the addition of the inert background salt (to maintain the ionic strength constant), the dissociation constants are modified. That is because the activity coefficient values vary with the change of the nature and the concentration of such salt Figs. 9S–12S depicts the dissociation constant of ligands as a function of the square root of the ionic strength, which was adjusted with KCl. An inspection of Tables 7–10 and Figs. 9S–12S reveals that there is a regular increase in the value of pK with increasing ionic strength of the medium, in agreement with that reported [40].

3.7.1.3. Effect of temperature on the ionization constants, the stepwise formation constant and the thermodynamic parameters. The standard enthalpy changes, ΔH°, for the dissociation of studied ligands were deduced from the slope of the plot of the pK^H versus $1/T$ Figs. 13S–16S. The corresponding standard free energy change, ΔG° and the standard entropy change, ΔS°, for such dissociations are calculated using the following well-known relationship:

$$\Delta G^\circ = -2.303RT\log K^H = 2.303RT\mathrm{p}K^H$$

$$\Delta G^\circ = \Delta H^\circ - T\Delta S^\circ$$

The calculated thermodynamic functions are recorded in Tables 7–10. Inspection of these values reveals that:

(1) pK_a values decrease with increasing temperature from 298 to 308 K, i.e., the acidity of ligands increase with increasing temperature. On the other hand, the stepwise stability constants decrease with increasing temperature indication that the complexation processes are unfavorable with increasing temperature.
(2) The positive values of ΔG° indicate that the dissociation processes are non-spontaneous process while the chelation has a spontaneous character as revealed by the negative ΔG° values.
(3) The negative values of ΔS° for dissociation and complex formation due to the increased order as a result of salvation process, i.e. the sum of total of the bound solvent molecules with the dissociated ligand is more than the originally accompanying the undissociated form [41].

Table 10
The dissociation constants of H_2PPY in 50% (V/V) dioxane–water and KCl at different temperatures and it's thermodynamic parameters.

μmol/L	Dissociation constant						Free energy change (ΔG) kJ mol^{-1}						Enthalpy change (ΔH) kJ mol^{-1}		Entropy change (ΔS) J mol^{-1} K^{-1}	
	298 K		303 K		308 K		298 K		303 K		308 K					
	pK_1	pK_2	pK_1	pK_2	pK_1	pK_2										
0.1	13.04	9.00	12.33	8.47	9.93	6.65	53.1	40.4	53.5	40.7	53.9	41.0	28.51	21.54	−82.54	−63.23
0.15	14.25	8.65	11.47	7.77	8.85	4.22	94.8	78.6	95.6	79.3	96.3	79.9	49.54	40.62	−152.0	−127.6
0.2	11.85	8.75	9.92	7.55	8.84	6.19	51.8	44.3	52.2	44.7	52.6	45.0	27.63	23.48	−80.94	−69.99

Table 11
The stability constants of Co(II) complexes in 50% (V/V) dioxane–water and KCl at different temperatures.

Compound	μmol/L	Dissociation constant					
		298 K		303 K		308 K	
		Log$K$1	Log$K$2	Log$K$1	Log$K$2	Log$K$1	Log$K$2
$[Co(PPS)(H_2O)_2](H_2O)$	0.1	13.13	9.80	12.33	9.35	10.5	3.25
	0.15	19.14	10.02	–	6.20	–	7.61
	0.2	11.01	8.14	12.20	7.45	10.12	5.93
$[Co(PBO)(H_2O)](H_2O)_2$	0.1	17.08	6.58	15.58	5.31	11.11	3.81
	0.15	19.08	9.36	–	9.07	15.95	11.00
	0.2	–	13.37	–	9.02	–	12.48
$[Co(HAPO)Cl(H_2O)_2](H_2O)$	0.1	18.87	8.38	14.51	7.88	13.67	5.67
	0.15	11.58	6.94	–	12.26	–	7.29
	0.2	–	10.19	–	7.86	–	7.89
$[Co(HPPY)Cl(H_2O)](H_2O)$	0.1	19.52	10.19	15.78	5.51	10.24	4.46
	0.15	7.13	–	10.29	–	10.24	6.34
	0.2	12.23	9.19	13.75	7.88	–	6.95

Table 12
Thermodynamic parameters of Co(II) complexes in 50%(V/V) dioxanel–water and 0.1 M KCl at different temperature.

Compound	Free energy change (ΔG) kJ mol^{-1}						Enthalpy change (ΔH) kJ mol^{-1}		Entropy change (ΔS) kJ mol^{-1} K^{-1}	
	298 K		303 K		308 K					
Co(II) + H_2PPS	−75.4	−56.7	−68.9	−38.4	−62.4	−20.1	−461.4	−1149.4	−1.3	−3.7
Co(II) + H_2PBO	−97.7	−35.9	−81.8	−38.4	−62.4	−20.1	−1048.3	−484.42	−3.2	−1.5
Co(II) + H_2APO	−107.5	−48.1	−93.9	−40.9	−80.4	−33.7	−913.7	−476.0	−2.7	−1.4
Co(II) + H_2PPY	−112.2	−58.3	−86.8	−42.3	−61.3	−26.4	−1629.4	−1006.6	−5.1	−3.2

(4) The positive values of ΔH° indicate that the ionization of ligands in aqueous solution are endothermic indicating that the ionization processes are favorable at higher temperatures. The negative values of ΔH° of the chelation processes indicating that the processes are exothermic revealing that the complexation reactions are favorable at lower temperature.

3.7.2. Determination of stability constants of complexes

The stability constant are evaluated from the formation curves drawn between n and pL, where n, is the average number of ligand attached per metal ion and pL is the free ligand exponent, n values can be calculated [42].

The calculated stability constant values are summarized in Table 11. From the data in the tables, one can notice that for all the studied complexes, $\log K_1 > \log K_2$, i.e., the vacant sites of the metal ion is more freely available for the binding of the first ligand than that of the second.

Figs. 17S–20S represent the formation curves ($\bar{n}$versus pL) of the studied metal ion–ligand mixtures. The metal–ligand stoichiometric ratios were confirmed by the analyses of the pH-metric titration curves. All metal ions form 1:1 and 1:2 (M:L) ratios in solution with the ligands under study as gathered from $\bar{n}$,where $\bar{n}$ values extend between 0 and 2.

Furthermore, the thermodynamic parameters, ΔH° and ΔS° were obtained by linear least square fit of pK against $1/T$ with an intercept equals $\Delta S^\circ/2.303R$ and a slope of $\Delta H^\circ/2.303R$ Figs. 21S–28S. The free energy (ΔG°) change due to the complexation can be estimated using the following relationships:

$$\Delta G^\circ = \Delta H^\circ - T\Delta S^\circ$$

The calculated thermodynamic functions are recorded in Table 12. An insight on the data reveals the following remarks:

1) The stepwise stability constants decrease with increasing temperature indication that the complexation processes are unfavorable with increasing temperature.
2) All ΔG° values are indication of spontaneous character of chelation.
3) The negative values of ΔS° indicate that the complexation processes entropically unfavorable.
4) The negative values of ΔH° suggest that the chelation processes are accompanied by generation of heat indicating that the processes are exothermic revealing that the complexation reactions are favorable at lower temperature.

4. Conclusion

A new series of thiosemicarbazides ligands and their Co(II) complexes, Figs. 2–5, were prepared. Geometry optimization and conformational analysis have been performed and the perfect agreement with spectral studies allowed for suggesting the exact structure of all studies complexes. The stability of complexes was explained and kinetic parameters (E_a, A, ΔH^*, ΔS^* and ΔG^*) of all the thermal decomposition stages have been evaluated using Coats–Redfern and Horowitz–Metzger methods. Finally, the protonation and formation constants were calculated using pH metric studies.

Appendix A. Supplementary data

Supplementary data associated with this article can be found, in the online version, at doi:10.1016/j.molstruc.2011.08.020.

References

[1] P. Bindu, M.R.P. Kurup, T.R. Satyakeerthy, Polyhedron 18 (1999) 321–331.
[2] M. Joseph, V. Suni, M.R.P. Kurup, M. Nethaji, A. Kishore, S.G. Bhat, Polyhedron 23 (2004) 3069–3080.
[3] D.S. Kalinowski, Y. Yu, P.C. Sharpe, M. Islam, Y.-T. Liao, D.B. Lovejoy, N. Kumar, P.V. Bernhardt, D.R. Richardson, J. Med. Chem. 50 (2007) 3716–3729.
[4] D.L. Klayman, J.P. Scovill, J. Bruce, F. Bartosevich, J. Med. Chem. 27 (1984) 84–87.
[5] R.P. John, A. Sreekanth, V. Rajakannan, T.A. Ajith, M.R.P. Kurup, Polyhedron 23 (2004) 2549–2559.
[6] S.K. Dutta, D.B. McConVille, W.J. Youngs, M. Chaudhuri, Inorg. Chem. 36 (1997) 2517–2522.
[7] Z. Lu, C. White, A.L. Rheingold, R.H. Crabtree, Inorg. Chem. 32 (1993) 3991–3994.
[8] M. Joseph, M. Kuriakose, M.R.P. Kurup, E. Suresh, A. Kishore, S.G. Bhat, Polyhedron 25 (2006) 61–70.
[9] A.E. Liberta, D.X. West, Biometals 5 (1992) 121–126.
[10] I.M. Bazova, R.G. Dubenkon, P.S. Pel'kis, J. Organ. Khimii 14 (1976) 195; I.M. Bazova, R.G. Dubenkon, P.S. Pel'kis, Chem. Abstr. 84 (1976) 105468w.
[11] L.G. Van Uitert, C. Hass, J. Am. Chem. Soc. 75 (1953) 3651–3654.
[12] N.L. Allinger, J. Am. Chem. Soc. 99 (1977) 8127–8134.
[13] HyperChem version 8.0 Hypercube, Inc., 2002.
[14] I.M. Bazova, R.G. Dubenkon, P.S. Pel'kis, J. Organ. Khimii 14 (1976) 195; I.M. Bazova, R.G. Dubenkon, P.S. Pel'kis, Chem. Abstr. 84 (1976) 105468w.
[15] D.K. Rastoh, K.C. Sharma, J. Inorg. Nucl. Chem. 36 (1974) 2219–2228.
[16] (a) S.K. Nag, D.S. Joarder, Can. J. Chem. 54 (1976) 2827–2831; (b) S.K. Sengupta, S.K. Sahni, R.N. Kapoor, Acta Chim. Acad. Sci. Hungary 104 (1990) 89; (c) R. Roy, M. Chaudhury, S.K. Mondal, K. Nag, J. Chem. Soc. Dalton Trans. 8 (1984) 1681–1687.
[17] A.P. Rebolledo, M. Vieites, D. Gambino, O.E. Piro, E.E. Castellano, C.L. Zani, E.M.S. Fagundes, L.R. Teixeira, A.A. Batista, H. Beraldo, J. Inorg. Biochem. 99 (2005) 698–706.
[18] A.P. Rebolledo, G.M. De Lima, L.N. Gambi, N.L. Speziali, D.F. Maia, C.B. Pinheiro, J.D. Ardisson, M.E. Cortès, H. Beraldo, Appl. Organomet. Chem. 17 (2003) 945–951.
[19] R.F.F. Costa, A.P. Rebolledo, T. Matencio, H.D.R. Calado, J.D. Ardisson, M.E. Cortès, B.L. Rodrigues, H. Beraldo, J. Coord. Chem. 58 (2005) 1307–1319.
[20] I.C. Mendes, J.P. Moreira, L.N. Speziali, A.S. Mangrich, J.A. Takahashi, H. Beraldo, J. Braz. Chem. Soc. 17 (8) (2006) 1571–1577.
[21] A.B.P. Lever, Inorganic Electronic Spectroscopy, second ed., Elsevier, Amsterdam, 1984. 479.
[22] S. Sagdinc, B. Koksoy, F. Kandemirli, S.H. Bayari, J. Mol. Struct. 917 (2009) 63–70.
[23] A.W. Coats, J.P. Redfern, Nature 20 (1964) 68–69.
[24] H.H. Horowitz, G. Metzger, Anal. Chem. 25 (1963) 1464–1468.
[25] M.S. Abu-Bakr, H. Sedaira, E.Y. Hashem, Talanta 41 (10) (1994) 1669–1674.
[26] D. Kara, M. Alkan, Talanta 55 (2001) 415–423.
[27] A. Broido, J. Polym. Sci. A-2 7 (1969) 1761–1773.
[28] K. Schwetlick, Kinetyczne Metody Badania Mechanizmow Reakcji, PWN Warszawa (1975).
[29] R.G. Mortimer, Physical Chemistry, Harcourt and Science Technology Company, Academic Press, San Diego, 2000.
[30] S.H. Guzara, Q.H. Jin, Chem. Res. Chin. Univ. 24 (2) (2008) 143–147.
[31] H.T.S. Britton, third ed., Hydrogen Ions, vol. I, Chapman and Hall, London, 1942.
[32] T. Taakeyama, F.X. Quinn, Thermal Analysis Fundamentals and Applications to Polymer Science, John Wiley and Sons, Chichester, 1994.
[33] P.B. Maravalli, T.R. Goudar, Thermochim. Acta 235 (1999) 35–41.
[34] K.K.M. Yusuff, R. Sreekala, Thermochim. Acta 159 (1990) 357–368.
[35] S.S. Kandil, G.B. El-Hefnawy, E.A. Baker, Thermochim. Acta 414 (2004) 105–113.
[36] Clavin, Wilson, J. Am. Chem. Soc. 67 (1945) 2003–2007.
[37] J. Bjerrum, Metal Ammine Formation in Aqueous Solution, P. Hasse and Son, Copenhagen, 1941.
[38] H.M. Irving, H.S. Rossotti, J. Chem. Soc. (1954) 2904–2910.
[39] A.A. El-Bindary, I.S. Shehatta, E.M. Mabrouk, Monatsh. Chem. 125 (1994) 373–384.
[40] M. Jelikic, D. Veselinovic, P. Djurdevic, Talanta 39 (1992) 665–670.
[41] M.G. Abd El-Wahed, S.M. Metwally, M.M. El-Gamel, S.M. Abd El-Haleem, Bull. Kor. Chem. Soc. 22 (2001) 663–668.
[42] A. Mcaulery, G.H. Nacollas, J. Chem. Soc. (1961) 2215–2221.